Zhao *et al. Advances in Bridge Engineering* (2022) 3:28
https://doi.org/10.1186/s43251-022-00072-z

Advances in
Bridge Engineering

TECHNICAL NOTE **Open Access**

Advances in modeling boundary layer turbulence and its effects on motion independent aerodynamic force of bridge decks

Lin Zhao[1,2*], Fengying Wu[1], Zhenbiao Liu[3], Aiguo Yan[3] and Yaojun Ge[1]

*Correspondence:
zhaolin@tongji.edu.cn

[1] State Key Lab of Disaster Reduction in Civil Engineering, Tongji University, Shanghai 200092, China
[2] Key Laboratory of Transport Industry of Wind Resistant Technology for Bridge Structures, Tongji University, Shanghai 200092, China
[3] Bridge Design & Research Institute, China Railway Siyuan Survey and Design Group Co., Ltd, Wuhan 430063, China

Abstract

Wind tunnel tests remain crucial to solving the wind-induced issues, such as buffeting. The turbulence impacts on the aerodynamic forces is vital to buffeting responses of a bridge, which has been neglected, for that traditional passive wind tunnel test simulations are mainly to perform smaller turbulence integral scale, compared with the reduced-scale similarity. A turbulence hybrid simulation device that integrates vibrating grids and active fans was proposed, realizing a detectable adjustment of the bi-directional pulse energy of the incoming turbulence. The simulation development of the active turbulence in the wind tunnel test was reviewed briefly firstly. To investigate turbulence influence on the aerodynamic forces, the pressure-measurement wind tunnel tests of typical bridge decks were carried out in active control wind tunnel. The impacts of different incoming turbulence on the aerodynamic force and buffeting response were furtherly discussed. Results revealed that the bi-direction (along-wind and vertical wind) influenced aerodynamic forces synergistically. Otherwise, turbulence integral scale strongly influenced aerodynamic characteristics, such as buffeting responses, notably, the buffeting responses obtained in active controlled wind tunnel would be reasonable for a safety evaluation of bridges under construction and operation.

Keywords: Active controlled wind tunnel, Bi-direction incoming wind, Spatial coherence, Turbulence integral scale, Buffeting response of the bridge

1 Introduction

The wind features of the atmospheric boundary layer (ABL) are determined by the average wind velocity profile, turbulence intensity, integral scale (Liu et al., 2020), power spectrum, etc. (Simu and Scanlan, 1986). Before breakthrough achievements are made in turbulence theory, wind tunnel tests will remain the major approach to solving wind engineering issues (Larose, et al., 1997), in which the simulation of the ABL is critical. Currently, the wind characteristic simulation of the ABL consists of passive and active simulation technologies (Cermak and Peterka, 1978; Cermark, 1995). The passive simulation technology, mainly the inserts grids, wedges, and roughness elements into the stream field (Nishi false, 1997, are shown in Fig. 1. Wedges and roughness elements were

Springer Open

© The Author(s) 2022. **Open Access** This article is licensed under a Creative Commons Attribution 4.0 International License, which permits use, sharing, adaptation, distribution and reproduction in any medium or format, as long as you give appropriate credit to the original author(s) and the source, provide a link to the Creative Commons licence, and indicate if changes were made. The images or other third party material in this article are included in the article's Creative Commons licence, unless indicated otherwise in a credit line to the material. If material is not included in the article's Creative Commons licence and your intended use is not permitted by statutory regulation or exceeds the permitted use, you will need to obtain permission directly from the copyright holder. To view a copy of this licence, visit http://creativecommons.org/licenses/by/4.0/.

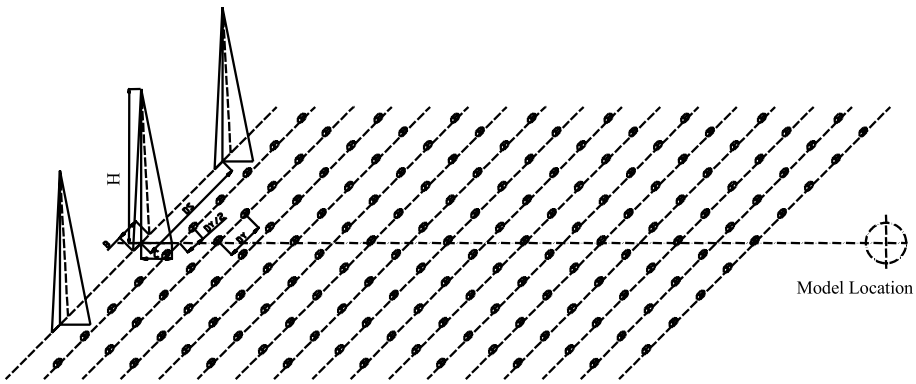

Fig. 1 Map of layout of the triangle wedges and roughness elements in the wind tunnel

first introduced in the simulation of the ABL wind field in the late 1960s (Lin and Wan, 1972). Various research results demonstrated that the wedges and roughness elements could produce appropriate wind profiles and large-scale turbulence and the turbulence intensity could be identical to the ABL (Kobayashi and Hatanaka, 1992; Kobayashi etal., 1994; Diana and Omarini, 2020).

This technology has been widely applied in the passive wind tunnel test of the ABL and its low cost and simple operation ensures that it is always used in wind tunnel tests for structures. This study simulated four types of uniform turbulent flows using passive grids. Figure 2 shows the wind spectrum function features of the turbulent flow, and Table 1 displayed the average fluctuation of turbulent flow.

The features of the turbulence field statistics generated from the passive measurements do not meet actual engineering demands, which increase daily. This defect is mainly due to the approach's small turbulence integral scale, which can only simulate the 1:300–1:500 boundary layer.

Compared to the passive wind tunnel, the active simulation technology (Kikitsu et al., 1999) mainly consists of vibrating grids, flanges or frequency-converting multiple fans, and more. The passive simulation mainly relies on the wake stream of the barrier to realize simulation, and it has limitations such as requiring the adjustment of wind spectrum intensity and turbulence integral scale (Ma et al., 2013). On the other hand, the active simulation employs a driving mechanism that injects random fluctuation energy into the wind tunnel. The simulation models perform their simulations on the turbulence field.

Additionally, the turbulence intensity is excessively attenuated in terms of height. The active simulation can appropriately increase the turbulence intensity and integral scale inside the wind tunnel, overcoming the technological defects of passive simulation (Teunissen, 1975; Bienkiewicz et al., 1983; Nishi et al., 1999). Moreover, the vibrating grid or multiple fans can enhance the simulation's along-wind turbulence intensity and integral dimension and introduce simulation errors in two directions (horizontal and downwind) or in more than three directions.

The active control wind tunnel was utilized to investigate how turbulence influence on the bridge aerodynamic performances, as the reason for turbulence impacted on aerodynamic forces is more important to wind-induced response. The development process of active control of generating turbulence was firstly briefly reviewed. Lately, it put forward with and designed the turbulence hybrid simulation device integrating the vibrating

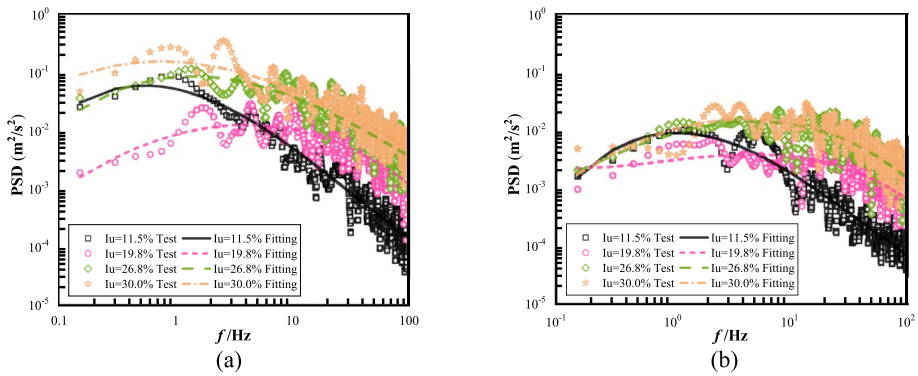

Fig. 2 Wind spectrum functions features of four kinds of turbulence flow fields (Incoming wind velocity is 5.3 m/s). **a** Wind spectral function at the along-wind direction. **b** Wind spectral function at the cross-wind direction

grids and active fans, and the adjustment of bi-directional fluctuating energy of incoming wind could be achieved. Accordingly, by combining the active wind tunnel pressure measurement tests on the typical bridge deck, furtherly analysed the difference of the wind spectrum energy of the incoming turbulence at the bending and the torsional fundamental frequency of the bridge. The results shown that the turbulence integral scale significantly influences buffeting responses of the bridge.

2 Active simulation of boundary layer turbulence

2.1 One-dimensional active control simulated turbulence

Figure 3 is the ABL wind tunnel from Colorado State University. The first active control simulation is the vibrating grid. The horizontally mounted active grid can enhance the vertical low-frequency spectrum energy with no influence on the downwind direction. Figure 4 shows comparisons of vertical power spectrum. Figure 4 (a) is the result measured from the static grid while Fig. 4 (b) is from the vibrating grid. These two figures indicated that the vibrating grid may lead to an energy increasement at the low-frequency region of the horizontal power spectrum.

Pertinent to the above problems, the modified ABL simulation is the multi-fan wind tunnel of the Miyazaki University of Japan (shown in Fig. 5). This simulation work based on a computer-controlled rotating frequency of the fans, realizing the actual simulation effects of the ABL by integrating winds of different frequencies. Unlike other simulations, it considers the time interval of the turbulence wind velocity when reproducing different statistical characteristic wind profiles. In addition, it well simulated the mutational wind and the interval turbulence.

Table 1 Average value of the fluctuating features of four kinds of flow fields (incoming wind velocity $\overline{U} = 4$ m/s-9 m/s)

Serial *No.*	I_u	I_w	L_u^x(cm)	L_w^x(cm)
1	11.5%	6.5%	20.17	11.97
2	19.8%	13.9%	25.52	17.45
3	26.8%	14.9%	30.61	14.51
4	30.0%	17.2%	34.98	16.25

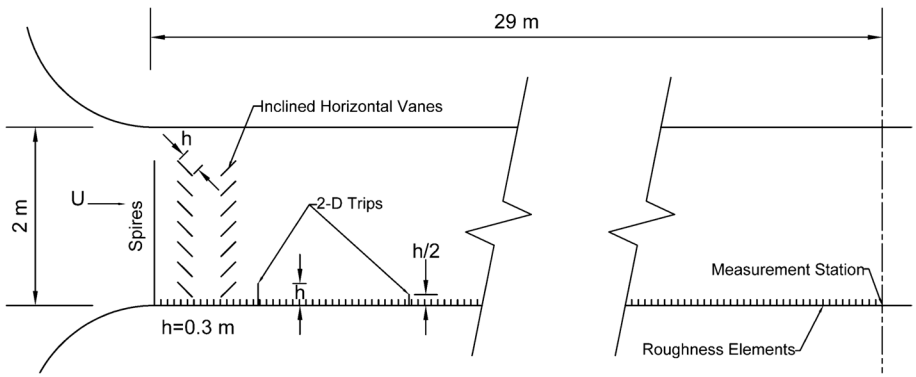

Fig. 3 Vibrating wing grid device of the atmospheric boundary layer (ABL) of Colorado State University

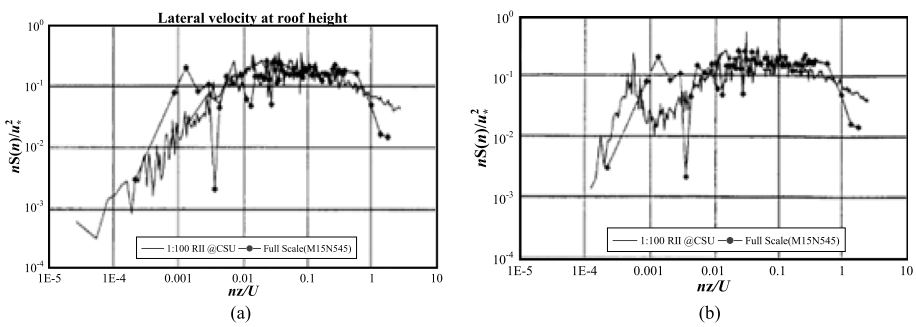

Fig. 4 Influence of the grid motion state to the vertical wind spectra function (Lin and Wan, 1972). **a** Static grid, **b** Vibrating grid

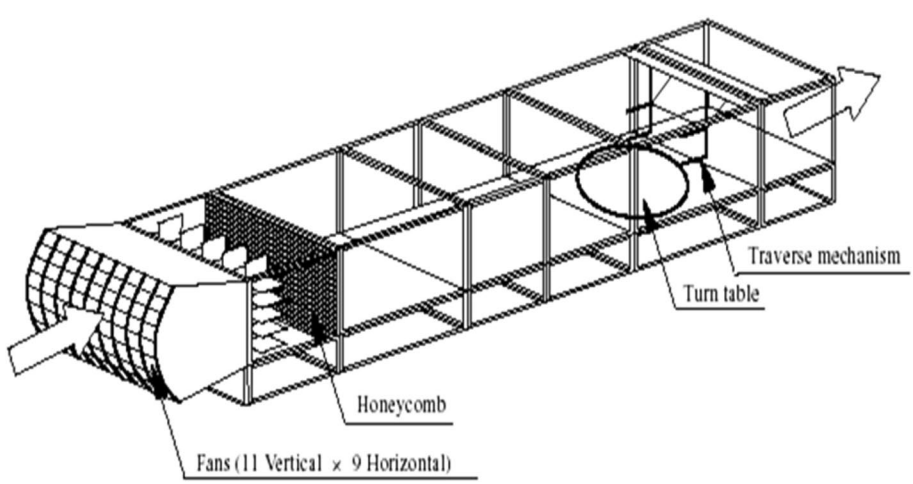

Fig. 5 Sketch map of the tri-dimensional multi-fan wind tunnel

Because the multi-fan generated the turbulence by the phase deviation among fans, they fail to produce sufficient along-wind and vertical wind turbulence. However, adding the vertical vibrating grids into the wind tunnel will enhance the longitudinal-vertical turbulence features. Thus, the multi-fan simulation alone can simulate the downwind features only. The multi-fan wind tunnel has well simulated the statistical wind features

of the turbulence, mutational wind, and interval turbulence and reproduced the wind time interval (Cao et al., 2002; Nishi and Miyagi, 1995). However, the multi-fan simulation on the ABL is restricted to the simulation on the downwind features because it cannot simulate the lateral or vertical direction and turbulence components can hardly reproduce the energy distribution relationship of the fluctuating wind in the lateral direction, as shown in Fig. 6.

The Wind Engineering Test and Research Center of Hunan University (Han, 2007) improved active grid technology by adding more small-size horizontal wings along the vertical direction at the entrance of the wind tunnel (shown in Fig. 7 a) and horizontal demarcation strips (shown in Fig. 7 b) between the horizontal wings. Thus, the horizontal wings could, during small-amplitude periodical angular movement (±15°), produce the cyclic pulsating flow simulation effect based on the open/closed grid theory. This device can generate the harmonic pulsating wind filed leading by single frequency with

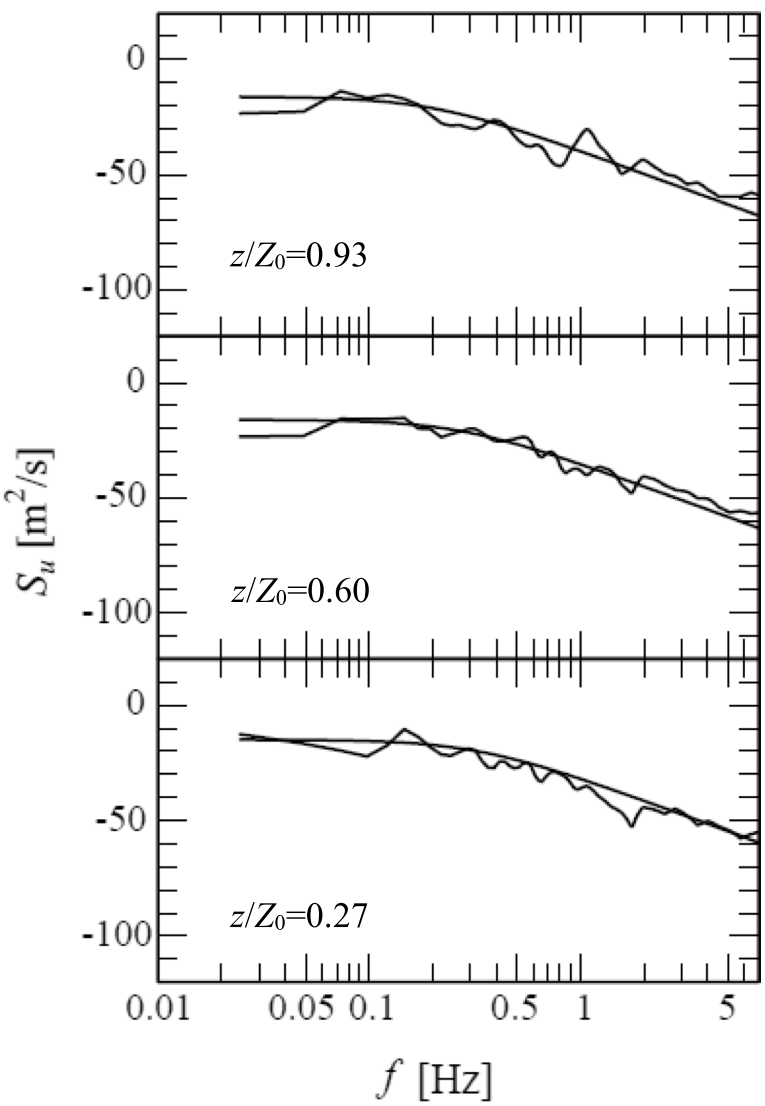

Fig. 6 Comparison of the power spectrum between the target and generated flows (Nishi et al., 1997)

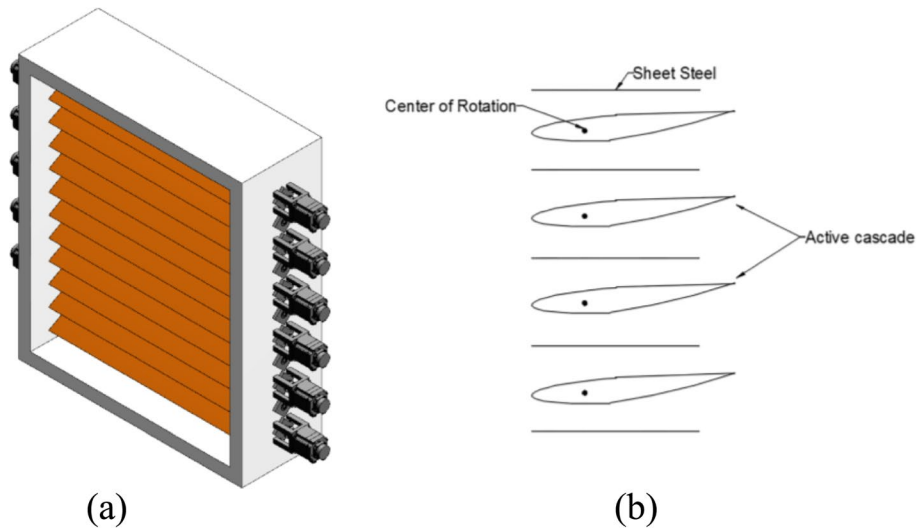

Fig. 7 Hunan University's Open/close grid device of the atmospheric boundary layer (ABL) **a** Layout sketch of the horizontal wings at the entrance of the wind tunnel. **b** Horizontal wings and horizontal demarcation strip (Han, 2007)

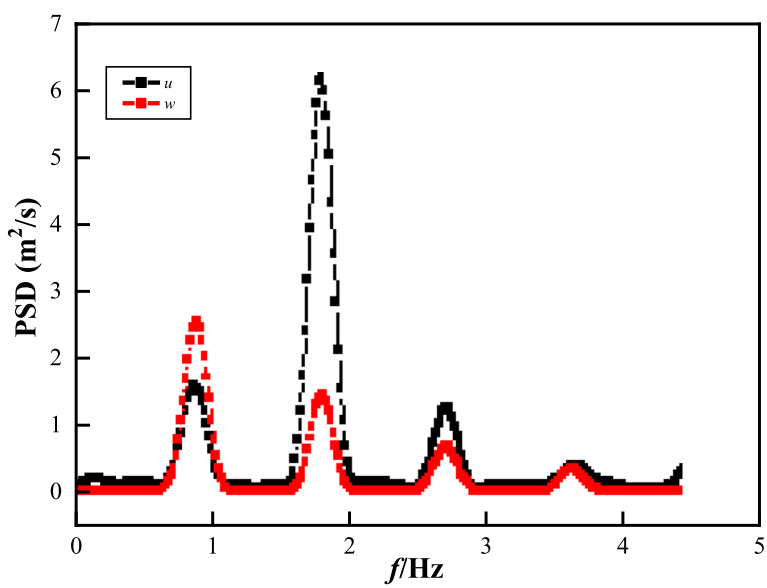

Fig. 8 Measured Fourier transform amplitude spectrum during the pulsating wind time interval (Han, 2007)

multiple along-wind and cross-wind relationships (shown in Fig. 8); here, the turbulence integral scale might reach more than ten meters, greatly enhancing the integral scale.

2.2 Two-dimensional active control wind tunnel

In summary, the vibrating grid and multi-fan active wind tunnel can simulate the energies of the two directions of the fluctuating wind. This paper designed and developed the turbulence simulation load device integrating the vibrating grid and active fan (shown in Fig. 9).

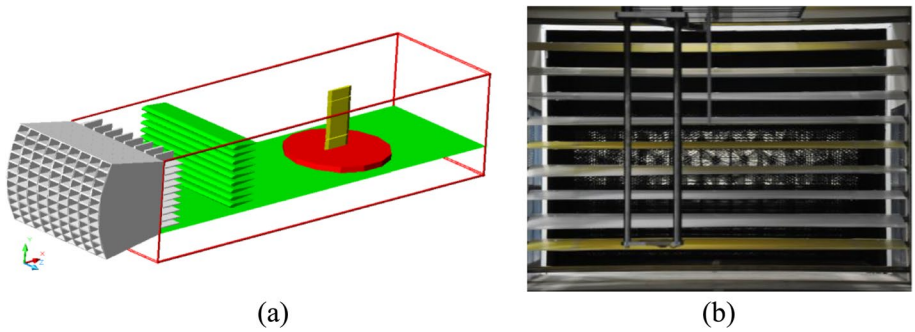

Fig. 9 Sketch of the combined vibrating-grid and active-fan turbulence simulation load device. **a** Tri-dimensional effects sketch. **b** Sketch of the installed equipment inside the wind tunnel

The multi-fan and vibrating grid wind tunnel could simulate the along-wind and cross-wind turbulence characteristics well, because the multi-fan and vibrating grid can obtain the along-wind and cross-wind features, respectively. The simulation of the average wind profile, turbulence intensity, integral scale, and power spectrum density complied with the target parameters. Furthermore, the Reynolds stress profile in the boundary layer was effectively simulated, and an almost constant value was obtained. Taking the single-frequency wind load for example, by adjusting the phase difference of the fan, grid, and the ratio between the frequency and energy amplitude, different combinational relations of the incoming turbulence energy of the two fluctuating winds can be regulated efficiently, as shown in Fig. 10.

3 Spatial characteristics of turbulence and aerodynamic force

To better understanding the spatial correlation of turbulence wind and aerodynamic force of bridge, the active control wind tunnel was adopted to simulate the turbulence wind, and the correlation of aerodynamic force was discussed under the fully correlation of turbulence wind condition.

In the time domain, the coherence of the pulsating wind is generally reflected by the autocovariance function. However, the self-correlation function cannot directly show the correlation degree, and thus, the correlation coefficient can be used. Taking the coherence of the vertical pulsating wind velocity at two different fixed points in the space at the same moment as an example ($v_1(r_1, \mathrm{t})$, $v_2(r_2, \mathrm{t})$), the pulsating wind component can be indicated by the cross-correlation coefficient as follows:

$$Cor(r_1, r_2) = \frac{\overline{v_1(r_1, t) \cdot v_2(r_2, t)}}{\sigma_{v1}\sigma_{v2}} \tag{1}$$

where σ_{v1} and σ_{v2} are the standard deviation of wind speed; $r1$ and $r2$ denotes two different fixed points at the same moment.

The coherence function is also mentioned as the frequency coherence coefficient; it is a function of the frequency and distance and defined as the absolute value of the normalized cross spectrum. The formula is as follow:

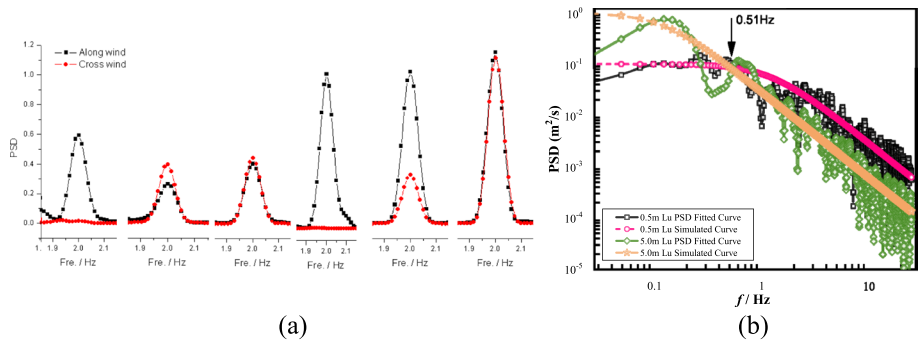

Fig. 10 Ratio of different energy amplitudes of adjustable fluctuating wind obtained from the combined turbulence simulation load conditions (Ma et al., 2013). **a** Adjustable fluctuating wind. **b** Different enery distribution

$$coh(f, \Delta y) = \frac{|C_{o12}(f)|}{\sqrt{S_{L_1}(f) S_{L_2}(f)}} \tag{2}$$

where f is the frequency and Δy is the distance between two points, $S_{L1}(f)$ and $S_{L2}(f)$ are the autocorrelation spectrum of the two time series, and $C_{o12}(f)$ is the cross-correlation function. For the buffeting, although the quadrature spectrum provides the phase angle, its spectrum is very small and can be ignored.

Davenport (1962), based on the measured data of the ABL, proposed an exponential relation of the spatial wind velocity:

$$coh_u(f, \Delta y) = \mathbf{exp}\left[-c\frac{f \cdot \Delta y}{\overline{U}}\right] \tag{3}$$

where c is the dimensionless attenuation constant and is generally the fitted value; $\overline{U}$ is the mean wind speed; Δy is distance between two points.

While handling the buffeting issues, the spatial coherence of the fluctuating aerodynamic force is replaced by that of the incoming turbulence and the spatial related function value root can be substituted by that of the wind velocity.

$$coh_L(\Delta y, f^*) \approx coh_w(\Delta y, f^*) \approx \mathbf{exp}\left[-C\frac{f \cdot \Delta y}{\overline{U}}\right] \tag{4}$$

The spatial function expression considers the frequency f, point-to-point distance Δy, wind velocity U, and other factors. This formula is simpler and has been used as the most common standard formula to address buffeting issues.

In a physical sense, the aerodynamic admittance function expresses the magnification of bridge deck force components for different frequencies of inflow wind dynamic action, or the mathematical corrections of the buffeting aerodynamic quasi-steady expression. It plays an important role in describing stochastic aerodynamics of structural sections under the action of fluctuating wind. For the cross section of a bridge girder, the common buffeting aerodynamic expressions are (Diana et al., 2010).

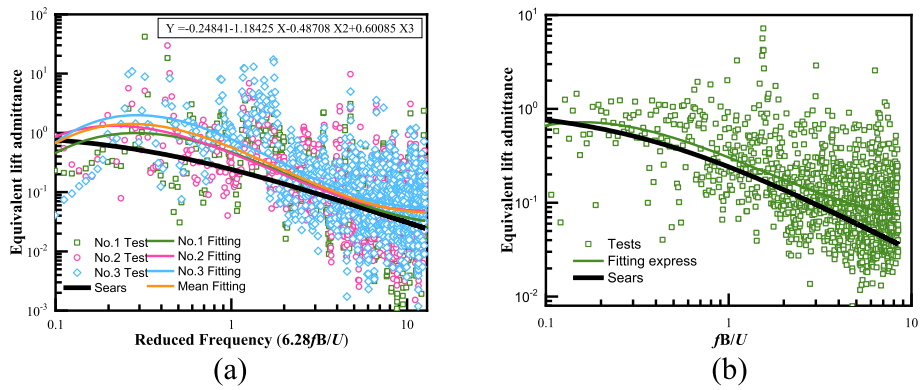

Fig. 11 Results of comparison between different methods of admittance recognition for streamlined box girder model under different integral scale (0° AOA, 11.5% turbulence intensity, and 5.3 m/s wind speed). **a** Recognition result of equivalent lift admittance function ($L_u^x = 3.0$ m). **b** Recognition result of equivalent lift admittance function ($L_u^x = 3.0$ m)

$$L_b(t) = \rho UB\left(C_L(\alpha)\chi_{Lu}u(t) + \frac{1}{2}\left(C_L{}'(\alpha) + C_D(\alpha)\right)\chi_{Lw}w(t)\right) \tag{5}$$

$$D_b(t) = \rho UB\left(C_D(\alpha)\chi_{Du}u(t) + \frac{1}{2}C_D{}'(\alpha)\chi_{Dw}w(t)\right) \tag{6}$$

$$M_b(t) = \rho UB^2\left(C_M(\alpha)\chi_{Mu}u(t) + \frac{1}{2}C_M{}'(\alpha)\chi_{Mw}w(t)\right) \tag{7}$$

where L, D, and M represent lift, drag, and torque components of the buffeting aerodynamic force per unit length, and show the relevant parameters of the aerodynamic items; ρ and U represent air density and inflow wind velocity, respectively; B is the bridge girder width; C is the static wind coefficient; C' is the derivative of static wind coefficient with respect to inflow angle of attack (AOA); χ is the aerodynamic admittance function; and u and w are the horizontal and vertical components of the fluctuating wind velocity, respectively. As subscripts, u and w are related to the wind component.

For simplicity, the analytical Sears function derived from the thin-plate or streamlined foil is usually used as the admittance function for a streamlined bridge deck (Diana et al., 2002; Zhao et al., 2020).

$$\chi_{Lu}(\omega) = \frac{S_w(\omega)S_{Lu}(\omega) - S_{wu}(\omega)S_{Lw}(\omega)}{\rho UBC_L(\alpha)[S_u(\omega)S_w(\omega) - S_{wu}(\omega)S_{uw}(\omega)]} \tag{8}$$

$$\chi_{Lw}(\omega) = \frac{S_u(\omega)S_{Lw}(\omega) - S_{uw}(\omega)S_{Lu}(\omega)}{1/2\rho UB\left[C_L'(\alpha) + C_D(\alpha)\right][S_u(\omega)S_w(\omega) - S_{uw}(\omega)S_{wu}(\omega)]} \tag{9}$$

$S_{wu} = \overline{S}_{uw}$ are complex conjugates and the cross-power spectrum of the u and w components of the turbulent wind velocities; S_{Lu} and S_{Lw} are the cross-power spectrums between the buffeting lift force and the u or w component of the fluctuating wind. For a comparison with the analytical Sears function admittance, the recognized

multi-component admittance functions should be converted into the so-call equivalent admittance function.

$$|\varphi_{LL}(K)|^2 = \frac{4C_L^2(\alpha)|\chi_{Lu}|^2 S_u(K) + \left(C_L'(\alpha) + C_D(\alpha)\right)^2 |\chi_{Lw}|^2 S_w(K)}{\left(4C_L^2(\alpha) S_u(K) + \left(C_L'(\alpha) + C_D(\alpha)\right)^2 S_w(K)\right)} \tag{10}$$

where $\left|\varphi_{LL}^2(K)\right|$ is the lift force equivalent admittance function, and in the same way, the two components of the resistance, torque aerodynamic admittance, and equivalent admittance function formula can be obtained, as shown in Fig. 11.

The comparison between the aerodynamic force spatial coherence of the typical closed box girder and the incoming turbulence coherence was obtained based on the active wind tunnel pressure-measuring test. The sectional model of the typical closed box girder was shown as Fig. 12, with a length of 1.4 m, a width of 0.476 m, and a height of 0.0357 m. End plates were adopted to avoid the influence of the three-dimensional flow of the model ends, as shown in Fig. 12. The pressure measurements were performed using a multi-channel pressure measurement system with PSI ESP-64HD miniature pressure scanners. A strip of 84 pressure taps was arranged in the middle section of the segment model surface, the pressure tap arrangement around the deck surface was displayed in Fig. 13. The sampling frequency was 200 Hz. The hot wire was adopted to capture wind speed

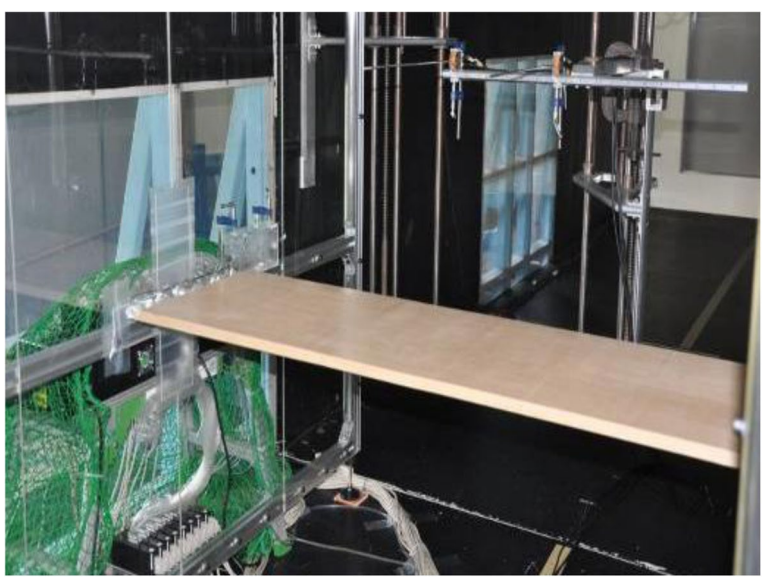

Fig. 12 Sectional model of pressure measurement test

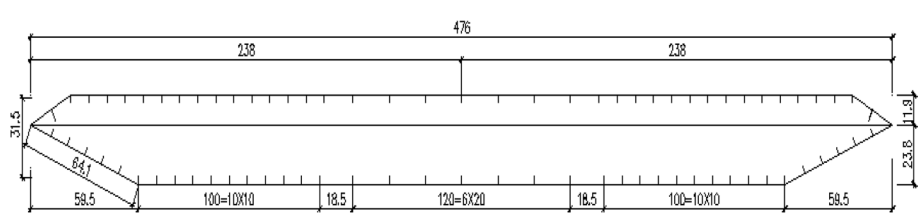

Fig. 13 Cross section of the model and pressure tube arrangement (unit: mm)

synchronously during the pressure-measurement test, the wind speed measurements were performed KANOMAX model1008 hot wire during experiments. The aerodynamic forces can be obtained by integral of wind pressures above model surface. During wind tunnel test, the characteristics of wind field was summarized as Table 2.

Figure 14 shows the incoming turbulence spatial coherence and aerodynamic force coherence results. The results indicated that the coherence of drag force was mainly influenced by along-wind. However, the impact of vertical wind has limited influence on the lift and moment forces. In general, the coherence of aerodynamic forces was both affected by the along-wind and vertical wind. The obtained aerodynamic force coherence was obviously greater than the coherence of the incoming turbulence, producing different results to traditional aerodynamic spatial coherence conclusions.

4 Turbulence integral scale and buffeting responses

This study used the segments models of the typical Chinese large-span suspension bridge (*A*), cable-stayed bridge (*B*), and arch bridge (*C*) as examples, performing calculations by using the buffeting frequency domain theory to compare and analyse the buffeting response root-mean-square value at two states: one was to calculate the buffeting response under the action of the fluctuating wind of the actual integral scale at the wind tunnel; and the others were to calculate the root-mean-square value under the bridge buffeting response under the turbulence integral scale given by the regulations (Zhou et al., 2010). Suspension bridge *A* gave two segment models under the two-scale ratio of 1:40 and 1:208. Tables 3 and 4 presented the design parameters and 3-D static component force coefficients of the three kinds of three segment models. However, the flutter derivatives of these segment models were beyond scope of this study.

In Table 3, suspension bridge *A* is a central slotting steel box suspension bridge with main span of 1650 m. Its stiff girder decks are made of the central slotting double-box girder with a full width of 36 m and the slotting width is 6 m. This study analysed the buffeting response of the 1:40 segmental model and the 1:208 full-bridge model of the suspension bridge. Analysis result showed the selection of the model scale ratio to the buffeting response when the turbulence scale at the wind tunnel was fixed. Cable-stayed bridge *B* is a steel box girder cable-stayed bridge with main span of 688 m and arch bridge *C* is a half-through arch bridge with a main span of 550 m. The bridges were used to discuss the effects of the general large-span bridge to the incoming turbulence integral scale. All these three bridges are located at the south-eastern coast of China, where there is a typhoon activity and random buffeting should be considered during their construction and operation.

Currently, widely accepted pulsating wind velocity spectrums include the Von Karman, Davenport, Simiu, and Harris spectra (Karman, 1948). All these spectra share

Table 2 Parameters of wind field

Serial *No.*	I_u (%)	Δy (m)	L_u (m)	U(m/s)	Δ/Lu
1	9.1	0.3	1.79	6.86	0.17
2	9.4	0.5	1.16	6.69	0.43
4	9.1	0.8	1.75	6.64	0.46

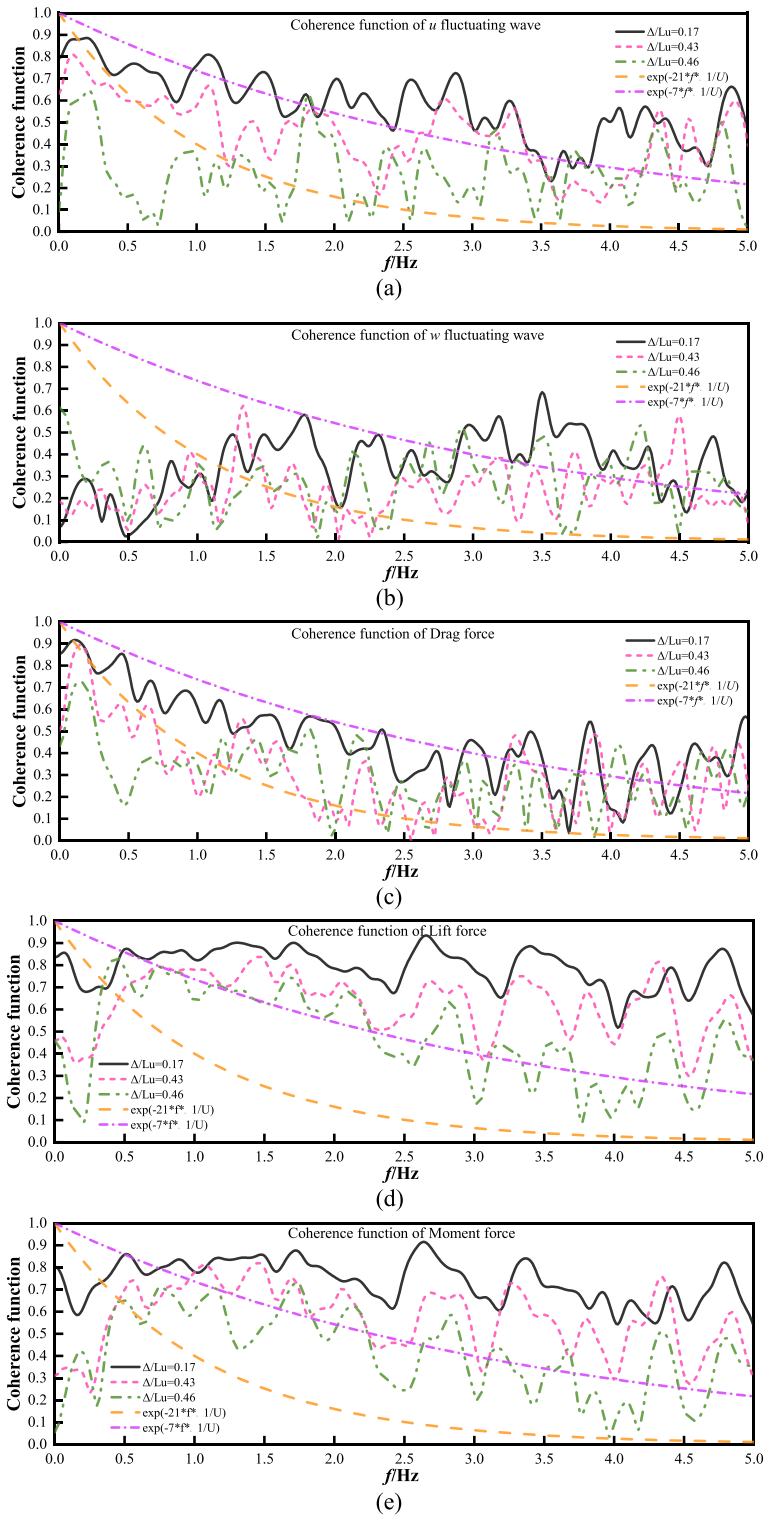

Fig. 14 Comparison between the aerodynamic force coherence and the incoming turbulence spatial coherence. **a** Curve of the along-wind velocity spatial related functions. **b** Curve of the vertical-wind velocity spatial related functions. **c** Curve of the Drag-force spatial related functions. **d** Curve of the Lifting-force spatial related functions. **e** Curve of the Moment-force spatial related functions

Table 3 Design parameters of the typical large-span bridge segment models

Parameters	Suspension Bridge *A*				Cable-stayed Bridge *B*		Arch Bridge *C*	
	Ratio of Similitude	Model	Ratio of Similitude	Model	Ratio of Similitude	Model	Ratio of Similitude	Model
Length L (m)	1:40	1.700	1:208	0.330	1:55	1.760	1:70	1.700
Width B (m)	1:40	0.900	1:208	0.170	1:55	0.618	1:70	0.560
Height H (m)	1:40	0.090	1:208	0.020	1:55	0.064	1:70	0.040
Equivalent Mass (Kg/m)	1:402	17.194	1:2082	0.636	1:552	8.473	1:702	7.942
Equivalent Mass Moments of Inertia (Kg. m^2/m)	1:404	1.564	1:2084	0.0022	1:554	0.231	1:704	0.309
Vertical bending frequency (Hz)	6.324:1	0.632	14.422:1	1.449	7.929:1	1.941	6:1	3.569
Torsional Frequency (Hz)	6.324:1	1.467	14.422:1	3.348	7.942:1	6.101	6:1	7.892
Wind Velocity Ratio (m/s)	1:6.324	–	1:14.422	–	1:6.935	–	1:11.67	–
Vertical Bending Damping Ratio	1.000	5.000	1.000	5.000	1.000	5.0	1.000	5.000
Torsional Damping Ratio	1.000	5.000	1.000	5.000	1.000	5.0	1.000	5.000

Table 4 The static force coefficients and derivatives of the 0°AOA of the typical large-span bridge segment models

Bridge segment model	C_D	$dC_D/d\alpha$	C_L	$dC_L/d\alpha$	C_M	$dC_M/d\alpha$
Suspension Bridge A	1.0176	−0.6303	−0.0375	1.8965	0.0169	0.3948
Cable-stayed Bridge B	1.0500	2.7130	−0.1443	2.5984	−0.0024	0.6159
Arch Bridge C	1.4300	−1.1459	−0.0990	7.7063	−0.0020	0.7735

some features and similar expressions but using different data sources for the spectra produced different expressions. The components of the Von Karman spectrum are physically significant, which can be similarly used by the horizontal and vertical wind spectrums. Therefore, this study adopted the Von Karman at the along-wind pulsating wind spectrum. Since the vertical Von Karman spectrum clearly shows the influence of the vertical turbulence integral scale, its defined as.

$$\text{The along-wind wind spectrum: } \frac{nS_u(n,z)}{u_*^2} = \frac{4\beta_u {f_u}^2}{\left(1+70.78{f_u}^2\right)^{5/6}}, f_u = nL_u^x/U(z) \tag{11}$$

$$\text{The vertical wind spectrum: } \frac{nS_w(n,z)}{u_*^2} = \frac{4\beta_w^2 f_w\left(1+755.2f_w^2\right)}{\left(1+283.2f_w^2\right)^{11/6}}, f_w = nL_w^x/U(z) \tag{12}$$

where L_u^x and L_w^x represent the along-wind and vertical turbulence integral scales, respectively; βu and β_ω are the friction velocity coefficient; and u^* is the friction velocity and here $\sigma_u^2 = \beta_u u_*^2$, $\sigma_w^2 = \beta_w u_*^2$. $U(z)$ shows the average wind velocity at the bridge deck height and is taken as the designed basis wind velocity at this height.

The wind tunnel measured results showed that the along-wind and vertical turbulence integral scales (L_u^x and L_w^x) of the segmental simulation tests were 0.3 m and 0.1 m, respectively. For the segmental simulations of the abovementioned bridges, the measured turbulence integral scales and the fluctuating wind spectrum input under the turbulence integral scales recommended by the specifications were used for the buffeting response calculation. The turbulence integral scale L_u^x of the horizontal fluctuating wind velocity u in the x direction can be found in the specifications for the wind-resistance design of the roads and bridges, while the turbulence integral scale L_w^x of the vertical fluctuating wind velocity w in the x direction has not been clearly expressed. Thus, according to the measured fluctuating wind features at the project site and considering the bridge deck height of these three bridges, the value of L_w^x was displayed in Table 5.

As the input of the buffeting response, the fluctuating wind spectrum is critical to the value of the buffeting response, displayed in Fig. 15. Each eddy scale in the boundary layer turbulence can be treated as a periodic fluctuation of frequency f has been triggered at that point. Since the fluctuating wind energy at the fundamental frequency of the bridge can be triggered most easily, we studied the fluctuating wind spectrum energy to analyse and compare the difference of the wind spectrum energy at the vertical bending fundamental frequency and the torsional fundamental frequency of the bridge, and thus, further explained the reasons for the buffeting response difference at different turbulence integral scales, as displayed in Table 6.

Table 6 presented that except for the suspension bridge A (1:40) model, all the along-wind spectrum values corresponding to the vertical bending fundamental frequency are larger in the wind tunnel calculation; and except for cable-stayed bridge B, all the cross-wind spectrum values corresponding to the vertical bending fundamental frequency are larger in the wind tunnel calculation. For the wind spectrum values corresponding to

Table 5 Comparison of different turbulence integral scales

Type of Bridge Segment	Bridge Deck Height (m)	Contraction Scale	Turbulence Integral Scale					
			Along-wind Direction L_U^X (m)			Vertical Direction L_W^X (m)		
			Actual Bridge	Model	Wind Tunnel	Actual Bridge	Model	Wind Tunnel
Suspension Bridge A (1:40)	62.56	1:40	120	3.00	0.30	60	1.50	0.10
Suspension Bridge A (1:208)	62.56	1:208	120	0.577	0.30	60	0.288	0.10
Cable-stayed Bridge B	55.85	1:55	120	2.182	0.30	60	1.091	0.10
Arch Bridge C	45.68	1:70	110	1.571	0.30	50	0.714	0.10

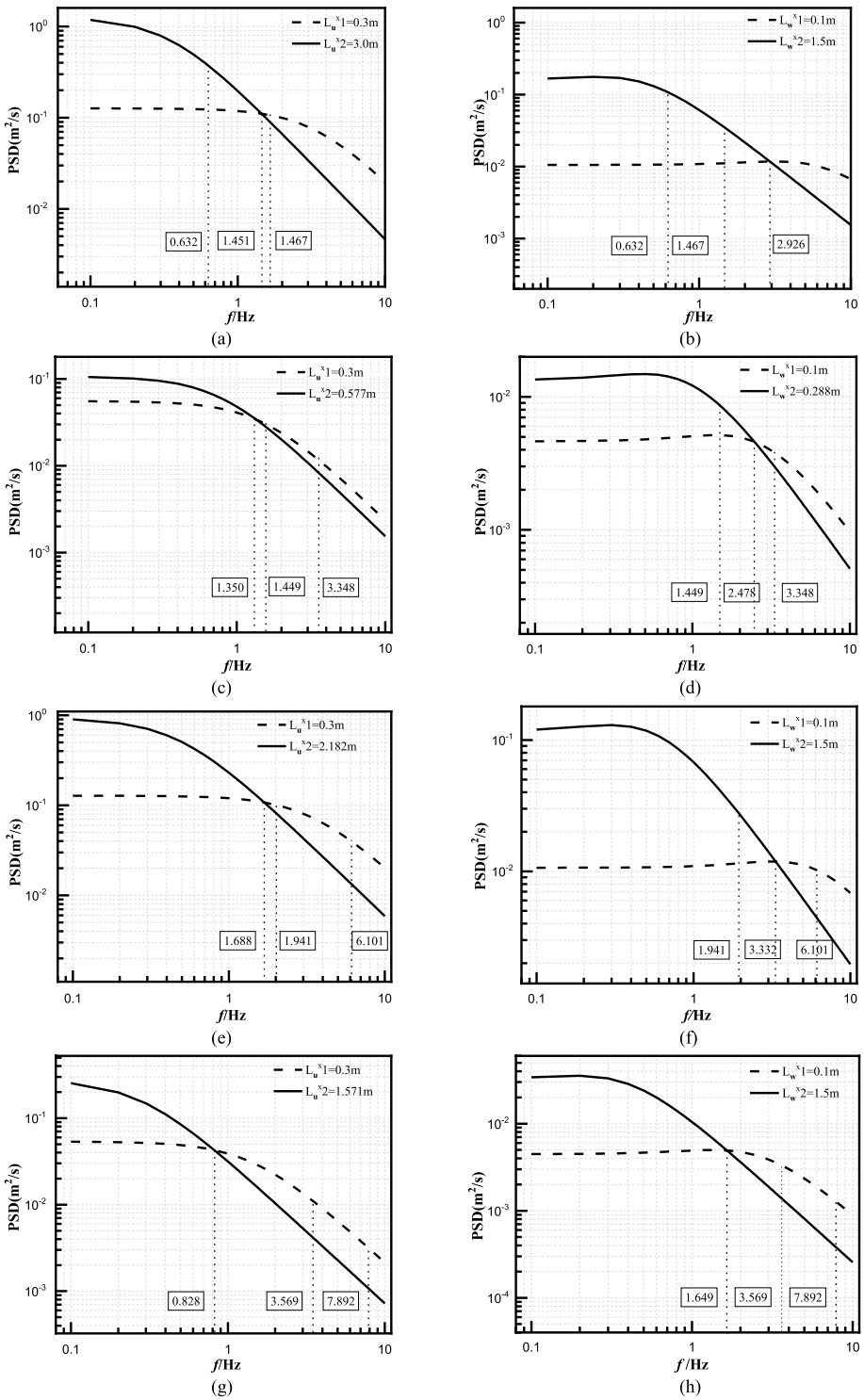

Fig. 15 Buffeting calculation results under different models and wind spectrum input conditions (Von Karman spectra). **a** Horizontal wind spectra for bridge *A* (1:40). **b** Vertical wind spectra for bridge *A* (1:40). **c** Horizontal wind spectra for bridge *A* (1:208). **d** Vertical wind spectra for bridge *A* (1:208). **e** Horizontal wind spectra for bridge *B*. **f** Vertical wind spectra for bridge *B*. **g** Horizontal wind spectra for bridge *C*. **h** Vertical wind spectra for bridge *C*

Table 6 Fluctuating wind power spectrum density under different turbulence integral scales

Segmental model of bridges	Wind spectrum input	Vertical bending fundamental frequency	Value of the fluctuating wind power spectrum density		Torsional fundamental frequency	Value of the fluctuating wind power spectrum density	
			Along-wind direction	Cross-wind direction		Along-wind direction	Vertical direction
Suspension Bridge *A* (1:40)	Wind Tunnel	0.632	0.123	0.011	1.467	0.106	0.011
	Actual Bridge		0.397	0.112		0.086	0.034
Suspension Bridge *A* (:208)	Wind Tunnel	1.449	0.030	0.288	3.348	0.011	0.004
	Actual Bridge		0.027	0.009		0.008	0.003
Cable-stayed Bridge *B*	Wind Tunnel	1.941	0.101	0.100	6.101	0.040	0.010
	Actual Bridge		0.082	1.091		0.014	0.004
Arch Bridge *C*	Wind Tunnel	3.569	0.011	0.003	7.892	0.003	0.001
	Actual Bridge		0.004	0.001		0.001	0.0004

the torsional fundamental frequency, we can see that except for the vertical wind spectrum of the suspension bridge *A* (1:40), the rest of wind spectrums are all larger in the wind tunnel calculation. These conclusions explain the calculation results of the buffeting response of the turbulence integral scales discussed later in this paper.

The buffeting response analysis was made to the three typical large-span bridges according to the calculation principle of the two-dimensional buffeting response (Zhao and Ge, 2009; Zhao et al., 2011), and the vertical displacement and torsional displacement root-mean-square values at the 0° AOA were obtained, as illustrated in Fig. 16, where the buffeting response of arch bridge *C* is the responsive root-mean-square value of the stiff girder. In the figure, "experimental" indicates the actual wind spectrum input of the wind tunnel while the "actual bridge" is the actual bridge wind spectrum input stipulated in the normative reference.

Generally, the model's fundamental frequency has a large buffeting response root-mean-square value for a high corresponsive wind spectrum energy. To be specific, the model's vertical bending fundamental frequency has a relatively large buffeting response root-mean-square value when its corresponsive wind spectrum energy is high and its torsional fundamental frequency has a relatively large buffeting response root-mean-square value for a high corresponsive wind spectrum. This phenomenon is more obvious under the wind velocity beyond the basis wind velocity. However, the changing directions of the horizontal and vertical wind spectra under the different integral scales corresponding to the same vertical bending frequency and torsional frequency are not always the same. The above analysis shows that under the 0° AOA, the changing direction of the buffeting response under different integral scales are identical with those of the energy of the horizontally fluctuating wind spectrum at the same integral scale, indicating that the horizontal fluctuating wind velocity u at the 0° AOA plays critical role to the buffeting response of the bridge.

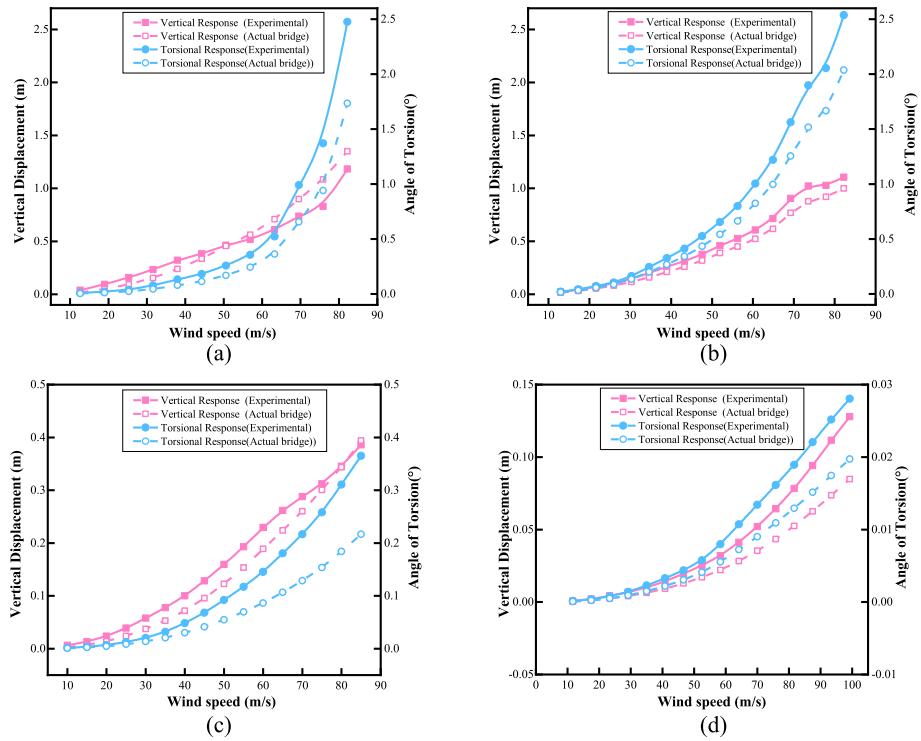

Fig. 16 Buffeting response root-mean-square values of the three typical bridges. **a** RMS value of bridge *A* (1:40). **b** RMS value of bridge *A* (1:208). **c** RMS value of bridge *B*. **d** RMS value of bridge *C*

Since the changing directions of the wind spectrum energy corresponding to the vertical fundamental frequency and torsional fundamental frequency under different integral scales are different, the changing directions of the buffeting vertical displacement and torsional displacement are not always the same. Taking the calculation results of the 1:40 model of suspension bridge *A* as an example, since the value of the horizontal wind velocity spectrum function corresponding to the vertical bending fundamental frequency of the model is large when $L_u^x = 3.0$ m while the value of the horizontal wind velocity spectrum function corresponding to the torsional bending fundamental frequency of the model is small; thus, under the condition that the wind velocity goes beyond the basis wind velocity, the buffeting vertical displacement of the bridge is large when $L_u^x = 3.0$ m, while the buffeting torsional displacement is small when $L_u^x = 3.0$ m.

Under different turbulence integral scales, the fluctuating wind power spectrum function may influence the structure response greatly at the points corresponding to the bridge's vertical and torsional fundamental frequencies. Thus, this study compared the relationship between the percentage of the energy difference and the corresponding buffeting response difference under the foresaid two integral scales; it also explained the influence of the turbulence integral scales to the buffeting response of different bridge structures from the viewpoint of the wind spectrum's energy input. Table 6 shows the fluctuating wind energy difference and buffeting response difference under different turbulence integral scales. In the table, the values of the wind spectra are the ones corresponding to the vertical and torsional bending fundamental frequency of the bridge model.

In the regular passive wind tunnel test, the integral scale is smaller than that of the incoming turbulence at the actual bridge location due to the restriction of the contraction scale. The difference percentage of the two values shown in Table 7 indicates the difference of the vertical and torsional displacement responses under the actual wind spectrum actions of the wind tunnel and at the bridge location stipulated in related specifications. Data in the table shows that for most of the bridge decks, due to the restriction of the turbulence integral scale simulation, the buffeting response result measured from the wind tunnel test under the basis wind velocity is bigger than the buffeting response results calculated based on the actual wind spectrum input. It indicates that for most conditions, the calculated buffeting responses at the passive wind tunnel were safe and the smaller integral scale at the passive wind tunnel can produce conservative analysis and conclusions. This conclusion is contradicts the belief that the dynamic load raised by the fluctuating wind at different parts is offset if the size of the pulsation vortex is smaller than that of the structure; thus, the obtained response value will be relatively small. Nevertheless, our results on the wind spectrum input energy under different turbulence integral scales show that the relatively high fluctuating wind spectrum input energy corresponding to the model's fundamental frequency contributes to the relatively large response caused by a small integral scale in the passive wind tunnel.

However, to some special large-span bridge decks, the wind tunnel model's buffeting response is still small. For instance, the vertical displacement buffeting response result of suspension bridge *A* (1:40) shown in Table 7 is equal to the change in direction of the fluctuating wind spectrum energy corresponding to the fundamental frequency shown in Table 6, indicating that the buffeting response obtained from the wind tunnel test may also have deviation from the site observation. Thus, the influence of the turbulence integral scale to the buffeting response should be amended and never be ignored.

The turbulence integral scale is a fixed value in the passive wind tunnel. For small-scale models (with a contraction scale from 1:400 to 1:600), the integral scale of the wind tunnel test is closer to that of the incoming turbulence at the actual bridge location. The two-dimensional buffeting research results obtained at the two scale ratios of suspension bridge A shows that since the actual integral scale of the passive wind tunnel under the small scale model is closer to reality, the buffeting response calculation result of the wind tunnel test has a smaller difference to the actual buffeting result and is higher than the buffeting response result of the actual incoming turbulence; thus, the calculation result is relatively safe. For the large-scale model (with a contraction scale from 1:20 to 1:40), the wind tunnel test result should be amended since the similarity of the turbulence integral scale deviates seriously from reality.

5 Conclusions

The impacts of turbulence on the aerodynamic forces of structure have been neglected more or less in previous studies, for that traditional passive wind tunnel test simulations are mainly to perform smaller turbulence integral scale meeting actual engineering demands. This study improved active turbulence simulation devices reproduce the actual bi-dimensional incoming turbulence impacted on aerodynamic forces, verifying and stressing the importance of sufficient bi-dimensional flow simulations for the aerodynamic forces.

Table 7 Differences of the wind power spectrum energy and the buffeting responses under different turbulence integral scales

Bridge	Response Type	Horizontal Wind Spectrum S_u			Vertical Wind Spectrum S_w			Buffeting Response at Basis Wind Velocity		
		S_{u1}	S_{u2}	$(S_{u1}-S_{u2})/S_{u2}$(%)	S_{w1}	S_{w2}	$(S_{w1}-S_{w2})/S_{w2}$(%)	Wind tunnel spectrum	Actual bridge spectrum	$(y_1-y_2)/y_2$ (%)
(1:40) Suspension Bridge *A* (1:40)	Vertical	0.123	0.372	−66.90	0.011	0.106	−89.90	0.517	0.562	−7.90
	Torsional	0.110	0.109	1.50	0.011	0.035	−68.20	0.355	0.244	45.70
(1:208) Suspension Bridge *A* (1:208)	Vertical	0.032	0.031	3.70	0.005	0.009	−42.00	0.526	0.451	16.80
	Torsional	0.013	0.009	38.50	0.004	0.003	28.10	0.799	0.662	20.70
Cable-stayed Bridge *B*	Vertical	0.102	0.086	18.50	0.012	0.028	−58.50	0.229	0.189	21.30
	Torsional	0.040	0.013	198.00	0.010	0.004	130.20	0.145	0.086	68.20
Arch Bridge *C*	Vertical	0.011	0.004	166.50	0.003	0.001	138.30	0.019	0.013	51.60
	Torsional	0.003	0.001	193.50	0.001	0.000	234.20	0.004	0.003	43.00

where S_{u1} and S_{w1} are experimental results; S_{u2} and S_{w2} are actual bridge results

The influence of the aerodynamic force spatial coherence on a structure's aerodynamic force were discussed; then, according to the full bridge tri-dimensional finite elements simulation results, the influence of the turbulence on the aerodynamic disability of the bridge structure was analysed. The conclusions were drawn as bellow.

(1) Limited by passive simulation of turbulence, this study put forward with a turbulence hybrid simulation loading device, which integrating the vibrating grids and the active fans. On this basis, bi-directional (along-wind and vertical wind) pulse energy of incoming turbulence were successfully simulated in active control wind tunnel.
(2) The turbulence impacted on the aerodynamic forces were furtherly discussed. Indicating that spatial coherence of aerodynamic forces was significantly affected by both along-turbulence and vertical turbulence. Additionally, the coherence of aerodynamic force was greater than the coherence of incoming wind, therefore, it also may influence wind-induced responses significantly.
(3) The relationship between the input energy and buffeting response differences under different integral scales were analysed. Results indicated that a high fluctuating spectrum input energy corresponds to the fundamental frequency of the model, revealing that the turbulence effect of the natural incoming turbulence might affect the aerodynamic performance of the bridge, and the large turbulence integral scale enhanced the buffeting responses.

Acknowledgements
The authors gratefully acknowledge the support of National Natural Science Foundation of China and Independent subject of State Key Lab of Disaster Reduction in Civil Engineering.

Authors' contributions
Lin Zhao conceived this study, participated in its design and coordination, and reviewed and revised the manuscript. Fengying Wu participated in the experiments, analysis of the test data, and drafting of the manuscript. Zhenbiao Liu, Aiguo Yan participated in the application promotion. Yaojun Ge conceived this study, participated in review this manuscript. All the authors read and approved the final manuscript.

Funding
This work was supported financially by the National Natural Science Foundation of China (52078383, 52008314) and Independent subject of State Key Lab of Disaster Reduction in Civil Engineering (SLDRCE19-B-11).

Availability of data and materials
The data and materials generated or used during the study are available from the corresponding author by request.

Declarations

Competing interests
Lin Zhao is an editorial board member for Advances in Bridge Engineering and was not involved in the editorial review, or the decision to publish, this article. The author(s) declared no potential conficts of interest with respect to the research, authorship, and/or publication of this article. Advances in Bridge Engineering.

Received: 26 September 2022 Accepted: 7 November 2022
Published online: 30 December 2022

References
Bienkiewicz B, Cermak JE, Peterka JA et al (1983) Active modeling of large-scale turbulence. J Wind Eng Ind Aerodyn 13(1–3):465–475
Cao SY, Nishi A, Kukugawa H et al (2002) Reproduction of wind velocity history in a multiple fan wind tunnel. J Wind Eng Ind Aerodyn 90:1719–1729
Cermak JE, Peterka JA (1978) Wind engineering applications to civil engineering. ASCE Convention and Exposition, Chicago

Cermark JE (1995) Wind-tunnel modeling of the atmospheric surface layer. J Wind Eng Ind Aerodyn 54(55):505–513
Davenport AG (1962) Buffeting of a suspension bridge by storm winds. J Struct Eng 88(ST3):233–268
Diana G, Bruni S, Cigada A et al (2002) Complex aerodynamic admittance role in buffeting response of a bridge deck. J Wind Eng Ind Aerodyn 90:2057–2072
Diana G, Omarini S (2020) A non-linear method to compute the buffeting response of a bridge validation of the model through wind tunnel tests. J Wind Eng Ind Aerodyn 201:104163
Diana G, Rocchi D, Argentini T, Muggiasca S (2010) Aerodynamic instability of a bridge deck section model: linear and nonlinear approach to force modeling. J Wind Eng Ind Aerodyn 98:363–374
Han Y (2007) Fine researches on the aerodynamic admittance function and buffeting of the bridge structure. Doctoral dissertation of Hunan University
Karman VT (1948) Progress in the statistical theory of turbulence. Proc Natl Acad Sci U S A 34(11):530–539
Kikitsu H, Kanda J, Iwasaki R (1999) Flow simulation by wind tunnel with computer-controlled multiple fans. J Wind Eng Ind Aerodyn 83:421–429
Kobayashi H, Hatanaka A, Ueda T (1994) Active generation of time history of strong wind gust in a wind tunnel. J Wind Eng Ind Aerodyn 53:315–330
Kobayashi H, Hatanaka A (1992) Active generation of wind gust in two-dimensional wind tunnel. J Wind Eng Ind Aerodyn 41(44):959
Larose GL, Tanaka H, Ginsing NJ et al (1997) Direct measurement of buffeting wind forces on bridge decks. J Wind Eng Ind Aerodyn 74-76:809–818
Lin SC, Wan CA (1972) Decay of isotropic turbulence generated by a mechanically agitated grid. The Physics of Fluids 15:1363–1369
Liu AQ, Cai CS, Han Y (2020) Time-domain simulations of turbulence effects on the aerodynamic flutter of long-span bridges. ABEN 1:7
Ma TT, Zhao L, Cao SY et al (2013) Investigations of aerodynamic effects on streamlined box girder using two-dimensional actively-controlled oncoming flow. J Wind Eng Ind Aerodyn 122:118–129
Nishi A, Kikugawa H, Matsuda Y et al (1997) Turbulence control in multiple-fan wind tunnels. J Wind Eng Ind Aerodyn 67&68:861–872
Nishi A, Kikugawa H, Matsuda Y (1999) Active control of turbulence for an atmospheric boundary layer model in a wind tunnel. J Wind Eng Ind Aerodyn 83:409–419
Nishi A, Miyagi H (1995) Computer controlled wind tunnel for wind engineering applications. J Wind Eng Ind Aerodyn 54(55):493–504
Simiu E, Scanlan RH (1986) Wind effects on structures, 2nd edn. Wiley, New York
Teunissen HW (1975) Simulation of the planetary boundary layer in a multiple-jet wind tunnel. Atmos Environ 9(2):145–174
Zhao L, Cao SY, Ge YJ, et al. (2011) Investigation of aerodynamic loading effects on typical streamline cross-section under active turbulence-generated conditions. *The 13th international conference on wind engineering*, July 10-15
Zhao L, Xie X, Cui W et al (2020) A novel forced motion apparatus with potential applications in structural engineering. J Zhejiang Univ-Sci A (Appl Phys & Eng) 21(7):593–608
Zhao L, Ge YJ (2009) Buffeting response sensitivity of multi-component aerodynamic admittance function of typical bridge deck. APCWE-VII the seventh Asia-Pacific conference on wind engineering, Taipei, Taiwan
Zhou YF, Zhao L, Ge YJ (2010) Analysis of the action of the turbulence integral scale to the buffeting response of the bridge. J Shock Vib 29(8):87–93

Publisher's Note

Springer Nature remains neutral with regard to jurisdictional claims in published maps and institutional affiliations.

Submit your manuscript to a SpringerOpen journal and benefit from:

- ► Convenient online submission
- ► Rigorous peer review
- ► Open access: articles freely available online
- ► High visibility within the field
- ► Retaining the copyright to your article

Submit your next manuscript at ► springeropen.com